Temperature Sensitivity Analysis of Inertial Measurement Unit Under Dynamic Conditions

Gabriele Patrizi, *Member, IEEE*, Marco Carratù, *Member, IEEE*, Lorenzo Ciani, *Senior Member, IEEE*, Paolo Sommella, *Member, IEEE*, Marcantonio Catelani, *Member, IEEE*, and Antonio Pietrosanto, *Senior Member, IEEE*

***Abstract*— In the modern technological world, there is a notable increase in the demand for precise sensors and sensing platforms in many different application fields. In the context of Industry 4.0, inertial measurement units (IMU) are now playing a central role in positioning estimation and anomaly detection, smart condition monitoring, and fault diagnosis tools. Despite this increasing development in recent years, the metrological characterization and sensor performances of inertial platforms still represent a current research gap. Currently, the actual dynamic operating conditions (e.g., temperature, humidity, and mechanical stress) endured by the device during its operating life are rarely considered in the literature. However, a thorough sensor characterization needs to consider all external stress sources. Trying to fill this research gap, this study presents the results of a measurement campaign conducted on a triaxial micro-electromechanical system (MEMS)-based IMU performed at different operating temperatures. The dynamic characterization has been carried out emulating the automotive field regarding both movements and operating temperatures. The analysis of the experimental results introduces specific metrics to quantitatively estimate the impact of the temperature dependence on the IMU measuring a repeatable movement.**

***Index Terms*— Automotive testing, inertial sensors, sensitivity analysis, sensor characterization, temperature dependence.**

I. Introduction

INDUSTRY 4.0 and internet of things (IoT) are nowadays strongly pushing forward toward the need for more sensors and sensing units [1], [2]. In many different industrial and manufacturing fields, the use of modern smart sensing platforms is increasing constantly as a support of many different purposes [3].

In this context, micro-electromechanical system (MEMS) stands out as a forefront technology in the field of sensing units, finding applications across diverse domains [4], [5]. The versatility of its features opens great opportunities for creating multiple sensor types, addressing a broad spectrum of requirements. A few examples of physical quantities that can be measured using MEMS-based sensors are pressure [6], acceleration [7], angular rate [8], magnetic field [9], temperature [10], humidity [11], presence of particular gases and/or chemical substances [12], sound intensity [13], and so on. Along with the low cost, the low power consumption, the high integration capabilities, and the great versatility, one of the main advantages of MEMS sensors is the low dimensions and weight, which allow to develop multisensor platforms capable of ensuring high performances satisfying multiple requirements. Inertial measurement units (IMU) represent a perfect example of such multisensor platforms that are spreading in different fields thanks to MEMS technology [14]. Usually, MEMS-based IMU integrates triaxial accelerometers, triaxial gyroscopes, and triaxial magnetometers to acquire data regarding the current positioning of the monitored object [15]. Examples of applications of MEMS-based IMU are unmanned aerial vehicles (UAVs), submarine vehicles, biomedical engineering, consumer electronics, manufacturing devices, robotic equipment, wearable devices, and human gesture recognition [16], [17]. In the automotive field, which is the topic of this work, MEMS-based IMUs are used in motorcycles, self-driving vehicles, electric vehicles, electric bicycles, and electric scooters for multiple purposes, such as [18], [19], and [20]:

1) automatic fault detection and isolation;
2) smart condition monitoring and condition-based maintenance;
3) prognostic and health management;
4) real-time decision-making;
5) optimization and control;
6) positioning estimation;
7) functional requirements.

Considering the increasing significance of MEMS-based IMUs, there is a critical need to examine their metrological characteristics and reliability [21]. Establishing proper metrological and reliability parameters is crucial to ensure the optimal system response throughout the entire life cycle, especially in harsh environmental conditions [22], [23]. Manufacturers often overlook the characterization of IMUs under external stress sources, neglecting mechanical, thermal,

Manuscript received 31 January 2024; revised 29 April 2024; accepted 30 April 2024. Date of publication 13 May 2024; date of current version 28 May 2024. The Associate Editor coordinating the review process was Dr. Lihui Peng. *(Corresponding author: Lorenzo Ciani.)*

Gabriele Patrizi, Lorenzo Ciani, and Marcantonio Catelani are with the Department of Information Engineering, University of Florence, 50139 Florence, Italy (e-mail: gabriele.patrizi@unifi.it; lorenzo.ciani@unifi.it; marcantonio.catelani@unifi.it).

Marco Carratù, Paolo Sommella, and Antonio Pietrosanto are with the Department of Industrial Engineering, University of Salerno, 84084 Fisciano, Italy (e-mail: mcarratu@unisa.it; psommella@unisa.it; apietrosanto@unisa.it).

Digital Object Identifier 10.1109/TIM.2024.3400332

or electrical stresses which are usually prevalent in practical applications. Consequently, it becomes a priority to study the metrological performances of sensors in the presence of these external stimuli. Recent literature highlights temperature excursions as a primary influencing factor on the functional and metrological performances of electronic devices of different types, spanning from power modules [24], sensors [25], IoT technologies [26], microcontrollers, and so on.

Trying to deal with temperature dependence, there are some works in recent literature proposing temperature compensation of a single MEMS sensor. For instance, polynomial-based temperature compensation of an MEMS accelerometer is proposed in [27], while temperature compensation of an MEMS gyroscope is proposed in literature following different approaches, such as backpropagation neural network [28], a combined genetic algorithm and neural network [29], a parameter-based interpolation [30], polynomial fitting [31], and an algorithm based on autoregressive moving average model [32]. However, despite the increase in the MEMS sensors market and the widely known negative effects of harsh temperature conditions on electronics, there still is a research gap in recent literature. Looking into this aspect more specifically, a full and detailed dynamic testing and characterization procedure of the entire IMU sensor under different operating temperatures, considering the real operating conditions that the IMU is forced to endure in the installation field, is not yet available.

To fill this gap, some preliminary research works available in [33] and [34] carried out a static characterization of several MEMS IMUs under temperature stress tests, focusing on the correlation between the IMU output and operating temperature. The previous papers pointed out a robust correlation measured across the IMU sensor outputs for each axis orientation and each sensor under examination. Such correlations have been discovered across multiple samples in static conditions, and they differ for every device in terms of sign and magnitude. Notably, the previous findings reveal also some miscalibration phenomena and loss of compensations (even when the operating temperature remains within the device's designated operating range). Interestingly, these minor temperature-induced miscalibrations appear to significantly impact the raw data acquired by the sensors, subsequently influencing the outcomes of common filtering algorithms employed in positioning applications. However, static characterizations can be misleading, as the device remains in a fixed position, measuring a constant input value throughout the entire test. This approximation is not always reasonable since devices actually need to monitor rapid movements when installed in a motorcycle or a car. In light of such limitations, there is a pressing need to introduce a new testing methodology to investigate the sensor's response dynamically, emulating the conditions encountered in the actual automotive field.

Therefore, building upon the experimental setup proposed for the dynamic characterization of IMU under vibration stress in [35], this article further extends the study, focusing on a temperature sensitivity analysis of IMU under dynamic conditions. In the previous research work [35], only mechanical stresses were involved. Instead, in this article, an additional characterization of an MEMS-based IMU under combined thermomechanical conditions is presented, illustrating the specific test plan and the customized experimental setup. The study of the sensor's response during the test (i.e., during the application of a dynamic combined temperature stress and controlled movement) allows quantitatively estimating the temperature dependence, introducing adequate performance evaluation metrics. The main contribution of this work is the development of a specific dynamic experimental platform able to emulate the automotive field of application in a controlled laboratory environment. Thermomechanical stress conditions are applied to the device under test (DUT), simultaneously inducing temperature stress and a controlled movement that needs to be acquired (i.e., dynamic temperature test). The experimental platform provides a laboratory simulation that realistically replicates the challenges faced by an MEMS sensor in practical scenarios when installed on terrestrial vehicles such as cars, motorcycles, or trucks. Hence, this research allows us to study the temperature dependence of the sensor's output and to provide a temperature sensitivity analysis without the necessity of setting up in-field measurement, which is a crucial point that currently both manufacturers and recent literature miss to consider. As a matter of fact, the introduction of dynamic characterization of the IMU sensors under different operating temperatures and the study of the sensor's response in a nonstandard environment is a crucial point not only in the automotive field (which is the topic of this article) but could also be extended to any other application environment where the sensors are forced to endure harsh operating conditions.

II. IMU Under Test: Main Features and Previous Assessment

The MEMS-based inertial unit considered in this work is a general-purpose IMU with nine degrees of freedom (DoFs), which means that the sensing platform acquires nine inertial quantities, namely, three accelerations (i.e., toward the *X*-, *Y*-, and *Z*-axes), three angular speeds (i.e., related to the movement across the *X*-, *Y*-, and *Z*-axes), and three magnetic field intensities (i.e., toward the *X*-, *Y*-, and *Z*-axes). The DUT is a relatively low-cost 16-bit MEMS platform that can be used for several applications according to the manufacturer's datasheet between −40 °C and 85 °C. The main metrological characteristics of the sensing platform are given as follows:

1) linear acceleration sensitivity of 0.732 mg/LSB at full scale (i.e., ±16 g);
2) sensitivity of the magnetic field intensity equal to 0.58 mG/LSB at full scale (i.e., ±16G);
3) angular rate sensitivity of 70 mdps/LSB at full scale (i.e., ±2000 dps).

No temperature drifts, nor temperature sensitivity-related parameters, are provided in the device's datasheet.

As mentioned in Section I, an initial static assessment was conducted to evaluate the performances of multiple DUTs when the operating temperature is nonstandard [33], [34]. Such previous studies pointed out unexpected and noteworthy temperature drifts on all the sensors embedded in the IMU.

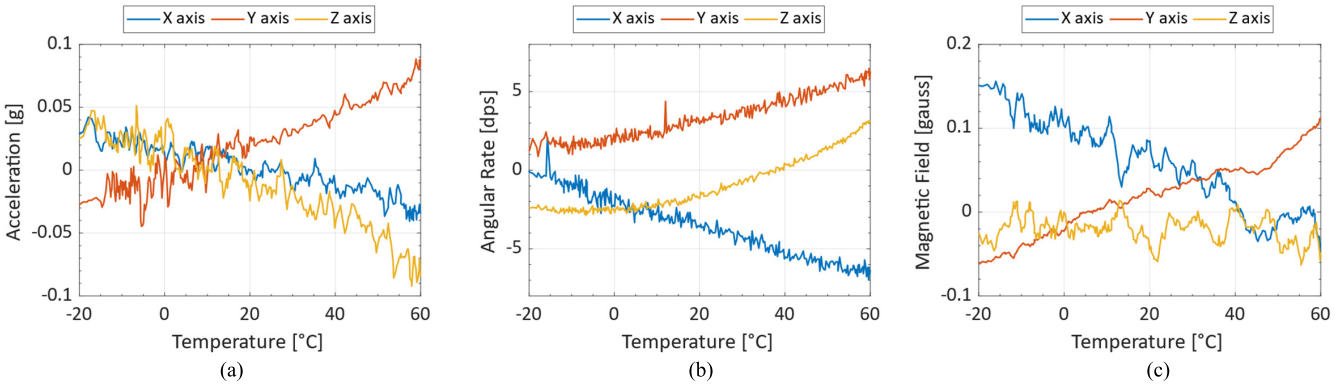

Fig. 1. Sensors output toward the *X*-, *Y*-, and *Z*-axes as a function of the operating temperature during a static test. (a) Accelerometer (gravitational acceleration has been removed from the sensor output). (b) Gyroscope. (c) Magnetometer.

TABLE I
QUANTITATIVE ANALYSIS OF THE IMU OUTPUT TEMPERATURE DRIFTS DURING A STATIC TEST

AXIS OUTPUT	ACCELEROMETER		GYROSCOPE		MAGNETOMETER	
	RANGE OF VARIATION	SLOPE OVER TEMPERATURE	RANGE OF VARIATION	SLOPE OVER TEMPERATURE	RANGE OF VARIATION	SLOPE OVER TEMPERATURE
X	0.083 g	-0.76 mg/°C	9.580 dps	-0.081 dps/°C	0.215 gauss	-2.22 mgauss/°C
Y	0.145 g	1.35 mg/°C	6.120 dps	0.061 dps/°C	0.194 gauss	1.98 mgauss/°C
Z	0.166 g	-1.40 mg/°C	6.710 dps	0.073 dps/°C	0.077 gauss	-0.29 mgauss/°C

For instance, Fig. 1 illustrates the output of a random IMU tested under static test conditions varying the operating temperature inside the device's specification between −20 °C and 60 °C. In particular, Fig. 1(a) shows the accelerometers' output toward *X*-axis (blue trend), *Y*-axis (red curve), and *Z*-axis (yellow line). Similarly, Fig. 1(b) involves the gyroscope outputs, while Fig. 1(c) illustrates the magnetometer outputs.

During the test, the IMU was held in a fixed position, and the temperature was increased from −20 °C up to 60 °C using a slow changing rate. Analyzing the figure, a remarkable temperature drift is evident across all three sensor types and all three sensor axes. Notably, the most remarkable finding is the distinct temperature drift observed for each axis, both in terms of direction and magnitude.

To numerically assess the temperature sensitivity during the static test, Table I illustrates the range of variation for the three axes of the accelerometer, gyroscope, and magnetometer, respectively. The table also presents the slope of the measured data calculated assuming a linear regression model in order to show the actual dependency between the IMU output and the operating temperature.

The most striking result to emerge from Fig. 1 and Table I is the divergence in the temperature drifts in terms of both magnitude and sign among the three sensor types and three sensor axes. Thus, the preliminary static analysis allowed to state that the temperature dependence is considerable and unpredictable, as it varies for each device and axis.

III. PROPOSED EXPERIMENTS: TEST PLAN AND TEST SETUP

This section illustrates the experimental campaign carried out in this work to extend the previous study and perform a dynamic characterization of the MEMS-based IMU under various operating conditions.

A. Test Plan for Dynamic Characterization of IMUs Under Temperature Stress

The main idea of the proposed dynamic test is the simultaneous application of a mechanical and thermal load to the IMU under consideration.

First, regarding the thermal load, a specific operating temperature is set in the interval T_{range} starting from −20 °C to 60 °C. The considered temperature range lays within the maximum operating range specified in the manufacturer datasheet. The significance of T_{range} is connected to the field of application of the sensors, which is supposed to be the automotive application. In this case, a temperature variation of 80 °C in the interval from −20 °C to 60 °C is reasonable assuming an installation outside the motor compartment.

All the subsequent tests are repeated in every operating temperature inside T_{range} assuming a temperature step of 5 °C. Such limited temperature increase allows for an accurate characterization of the sensor's temperature dependencies.

Regarding the mechanical load, a specific movement is forced during the test to emulate an actual motorcycle application. This particular motion involves two rotational axes: PAN, representing horizontal movement, and TILT, representing vertical movement. The speed and acceleration of the rotations are designed and controlled to ensure the maximum fluidity of the whole movement.

For the sake of generality and according to the physical constraints of the equipment to be used, the two mechanical movements follow the steps illustrated in the diagram in Fig. 2.

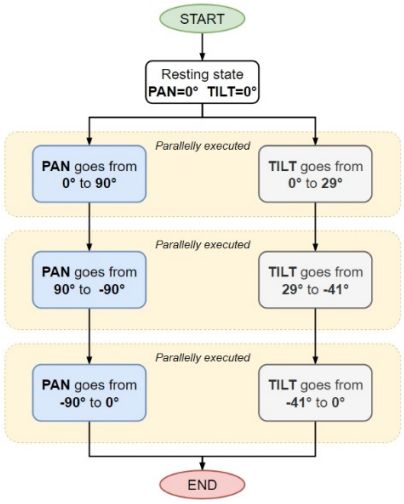

Fig. 2. Flowchart of the development movement around PAN and TILT axes of rotation.

The schematic reported in Fig. 2 shows different color movements performed according to PAN and TILT axes, highlighting the rotations that have been executed simultaneously. Analyzing the movements in detail, it is possible to identify two parallel tasks.

1) A symmetric movement spanning 180° is performed in the PAN rotation axis. It starts reaching 90° position from the resting state (i.e., 0°). For the sake of symmetry, the direction is then reversed toward –90° before changing direction again in order to return to the initial rest position. This rotation is performed at speed and acceleration equal to 115 and 123 $^\circ/s^2$, respectively.
2) A nonsymmetric movement spanning 70° is performed in the TILT rotation axis. It starts reaching 29° position from the resting state before changing direction reaching –41°. Finally, the movement involves another direction swift finishing in the rest position. This rotation is performed at speed and acceleration equal to 82 and 103 $^\circ/s^2$, respectively.

The movement in Fig. 2 is repeated 30× for the sake of repeatability, allowing a robust temperature sensitivity analysis.

B. Experimental Setup

The experimental setup required to implement the test plan in Section III-A is illustrated in Fig. 3. More specifically, the complete setup is shown in Fig. 3(a), while a detail of the tested IMU mounted on a moving device is reported in Fig. 3(b) for a better understanding. The main equipment is the pan-tilt unit (PTU), which is an electromechanical controllable device that generates stable, reproducible, and controllable movement toward two rotation axis (i.e., PAN and TILT rotations). Because of physical constraints, the maximum aperture angle of the TILT is limited, leading to a customized nonsymmetric movement included in the test plan as described in Section III-A.

A dedicated controller and a specific Python framework are used to set the PTU and ensure a real-time position check.

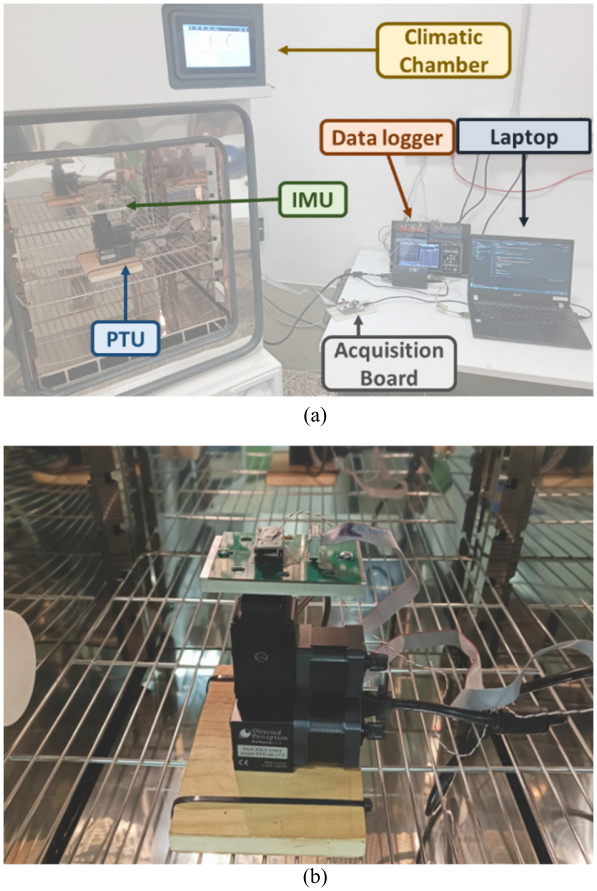

(a)

(b)

Fig. 3. Experimental equipment for dynamic thermomechanical test. (a) Complete experimental setup. (b) IMU mounted on the PTU.

The IMU is mounted on top of the PTU using a suitable metallic plate and hosting printed circuit board (PCB). The IMU and the PTU are then located inside a climatic chamber, which has been used to regulate the operating temperature in the specified range. A data logger equipped with a T-type thermocouple has been used to measure the overheating of the IMU platform during the test, while the temperature regulation during the test and the cohesion with the test plan is managed by the climatic chamber internal resistance temperature detector (RTD). Finally, an acquisition board based on a Nucleo 64 by STMicroelectronics is used to set the sensors and acquire the inertial data, which are then stored in the laptop.

IV. Temperature Sensitivity Analysis

This section presents the temperature dependencies of the IMU sensors during a dynamic test, considering the experiments proposed in Section III to emulate the automotive field of application.

To ensure a robust temperature sensitivity analysis, all the following discussions and considerations are referred to the average values of the 30 identical test repetitions performed for every operating condition.

A general overview of all the acquired data is presented in Fig. 4, considering the X-axis (blue shaded area), Y-axis (red shaded area), and Z-axis (yellow shaded area) of the

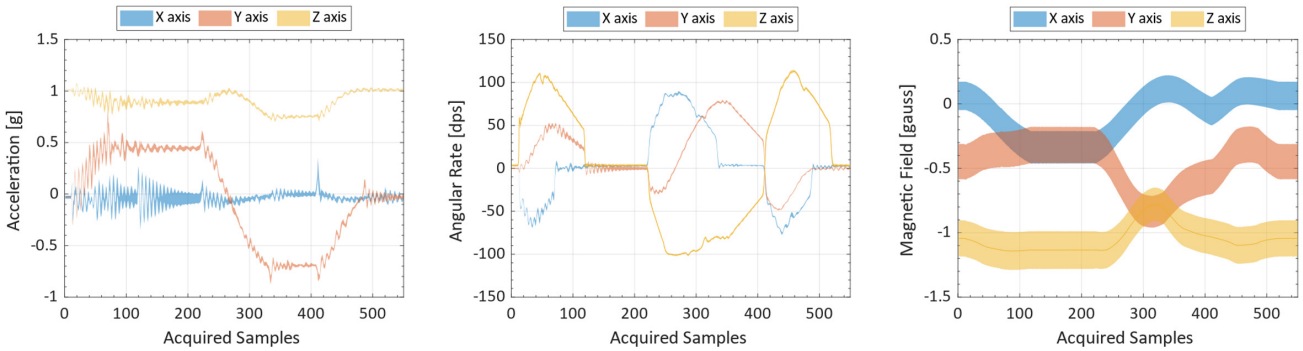

Fig. 4. Sensors output toward the X-, Y-, and Z-axes acquired at different operating temperatures as a shaded area around the average value. (a) Accelerometer. (b) Gyroscope. (c) Magnetometer.

accelerometer [Fig. 4(a)], gyroscope [Fig. 4(b)], and magnetometer [Fig. 4(c)]. For the sake of compliance, also the following figures have the same division of the subplots to identify the sensors and the same color code to identify the axes.

In Fig. 4, all the sensor's data acquired at different temperatures have been reported as a shaded area around the reference condition (i.e., $T = 20$ °C). What stands out from all the subplots in Fig. 4 is a general dispersion of the data caused by the changing operating conditions (i.e., changing the operating temperature from $T = -20$ °C to $T = 60$ °C). However, the three sensors exhibit different output variations due to the operating temperature. The maximum temperature impact seems to be endured by the three axes of the magnetometer, while a minor effect is exhibited on the gyroscope. The accelerometer shows intermediate variations caused by the temperature changes, with maximum effect located around the areas at constant acceleration.

Qualitatively speaking, another thing that comes out from the figure is the significant extension of the shaded areas in the case of the magnetometer, while the accelerometer and gyroscope seemed to show a less noticeable deviation. However, this is mainly due to the high vertical dynamics of both accelerometer and gyroscope during the proposed movement, which does not allow to properly appreciate the data dispersion caused by temperature for these sensors.

Thus, due to such a high dynamic of the gyroscope and accelerometer, it is better and more straightforward to analyze this aspect, focusing only on a subset of the proposed movement.

In this regard, Fig. 5 illustrates the output variations measured by the sensors at $T = -20$ °C (black curves), $T = 20$ °C (green curves), and $T = 60$ °C (dark red curves) focusing only on the central part of the movement for the X-axis of the accelerometer [Fig. 5(a)], Y-axis of the gyroscope [Fig. 5(b)], and Z-axis of the magnetometer [Fig. 5(c)]. The specific time interval (i.e., samples 250–350) has been chosen randomly over the entire test duration. Similar considerations can be drawn, moving the window frame used in Fig. 5 toward the beginning or the end of the test. All subplots of Fig. 5 show a nonnegligible offset of the sensors' output caused by the different operating temperatures. This finding is noteworthy, especially because the operating temperature during the test has always been kept within the maximum operating conditions allowed by the manufacturer. Another important aspect pointed out in Fig. 5 is the different signs of the temperature drifts for the three sensors embedded in the IMU under test. More specifically, the X-axis of the accelerometer experiences an increase in the temperature drift when the operating temperature decreases.

A similar behavior is pointed out also by the Y-axis of the gyroscope, while the magnetometer suffers from a directly proportional temperature drift that increases the sensor output when the temperature increases. However, analyzing all sensors' output, the different axes of the same sensor could experience opposite temperature drifts.

This aspect can also be appreciated by analyzing Fig. 6, where the 3-D reconstruction of the sensors' output measured at three different operating temperatures is illustrated for the accelerometer in (a), the gyroscope in (b), and the magnetometer in (c). Therefore, to further analyze this aspect, the sensor's offset caused by the different operating temperatures has been evaluated for all the test conditions.

First, let us consider a^j_{ref}, ar^j_{ref}, and m^j_{ref} the array of the measured data along the j-axis at $T = 20$ °C from the accelerometer, gyroscope, and magnetometer, respectively.

Then, $O^j_{\text{Acc}}|_{@T_{\text{op}}}$ represents the accelerometer's offset along the j-axis at a temperature T_{op} and it is evaluated as the average value of the point-by-point difference between the acceleration measured along the j-axis at temperature T_{op} and the above-defined reference value a^j_{ref} across the entire movement (with N_{mov} identifying the number of samples acquired during a single test)

$$O^j_{\text{Acc}}\Big|_{@T_{\text{op}}} = \frac{1}{N_{\text{mov}}} \sum_{i=1}^{N_{\text{mov}}} \left(a^j_{T_{\text{op}}}(i) - a^j_{\text{ref}}(i) \right). \tag{1}$$

Similarly, $O^j_{\text{Gyro}}|_{@T_{\text{op}}}$ and $O^j_{\text{Mag}}|_{@T_{\text{op}}}$ represent the offset evaluated at a temperature T_{op} along the j-axis of the gyroscope and magnetometer, respectively, and they are defined as

$$O^j_{\text{Gyro}}\Big|_{@T_{\text{op}}} = \frac{1}{N_{\text{mov}}} \sum_{i=1}^{N_{\text{mov}}} \left(ar^j_{T_{\text{op}}}(i) - ar^j_{\text{ref}}(i) \right) \tag{2}$$

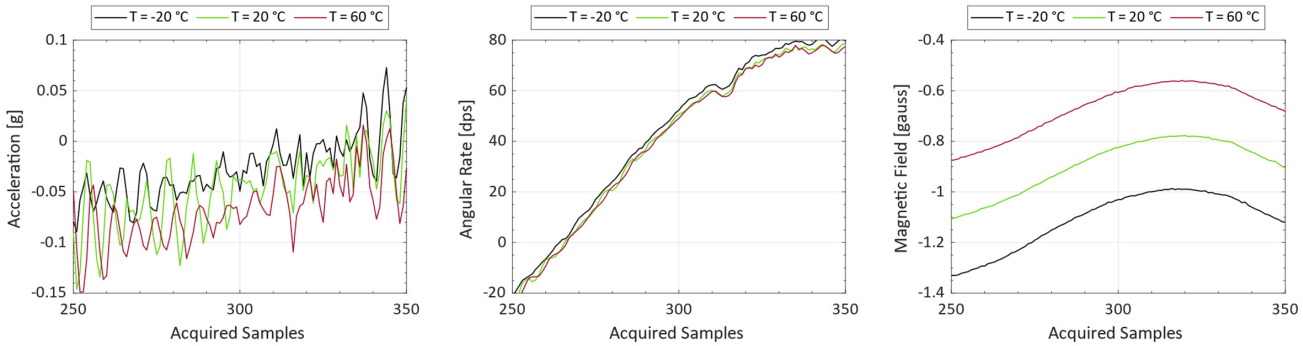

Fig. 5. Sensors output toward at three different operating temperatures in the central part of the movement. (a) Accelerometer X-axis. (b) Gyroscope Y-axis. (c) Magnetometer Z-axis.

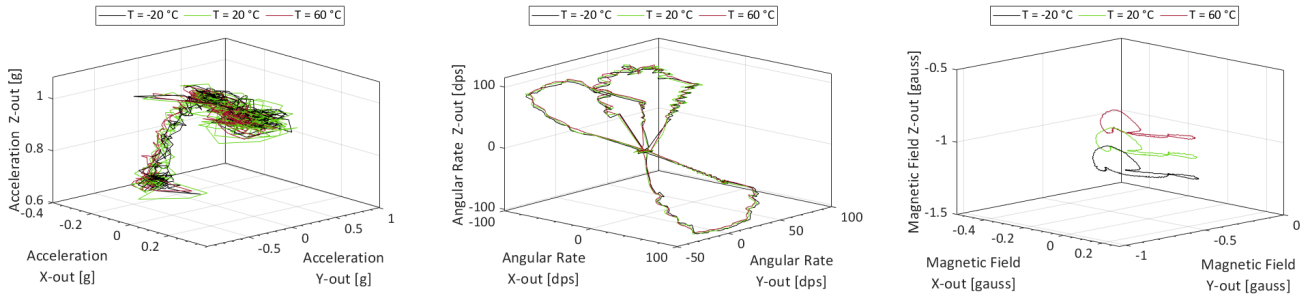

Fig. 6. 3-D-reconstruction of the measured data at three different operating temperatures. (a) Accelerometer. (b) Gyroscope. (c) Magnetometer.

$$O^{j}_{\text{Mag}}\Big|_{@T_{\text{op}}} = \frac{1}{N_{\text{mov}}}\sum_{i=1}^{N_{\text{mov}}}\left(m^{j}_{T_{\text{op}}}(i) - m^{j}_{\text{ref}}(i)\right). \tag{3}$$

The specific offsets estimated following (1)–(3) are illustrated in Fig. 7 as colored markers for every sensor [accelerometer in (a), gyroscope in (b), and magnetometer in (c)] and every axis. Furthermore, Fig. 7 also includes the linear fitting of the estimated temperature offsets, pointing out a strong linear dependence on all sensors and all axes between the temperature and the measured output. What stands out from Fig. 7(a) is that the X-, Y-, and Z-axes of accelerometer have different offsets in terms of magnitude, but they all agree in terms of sign, with an increment of the temperature drift when the operating temperature decreases. Instead, Fig. 7(b) and (c) proves the controversial behavior of the gyroscope and magnetometer.

The Y-axis of both sensors experienced a negative drift when the temperature increases, while the output of the X-axis and Z-axis of both gyroscope and magnetometer increased in accordance with temperature.

To summarize all these aspects, the temperature sensitivity (i.e., the slope of the linear fitting) of all sensors and all axes is reported in Table II along with the coefficient of determination R^2, which was taken as goodness of fitting metric. Furthermore, the table also includes the maximum swing experienced by the evaluated offset in the temperature range between -20 °C and 60 °C. The table once again demonstrates the different magnitudes and different signs of the temperature offset during the dynamic test. This means that dedicated and customized temperature compensation procedures are required for every sensor and every axis. Furthermore, comparing Tables I and II, it is possible to note that different temperature dependencies are experienced. This is because the preliminary static characterization and the proposed dynamic test have been carried out on different IMUs. Thus, the uncorrelated behavior (in terms of sign and magnitude) of the sensors' axes differs also depending on the specific DUT (for more test repetitions and more devices under static condition, see [33], [34]). To further proceed the analysis, another phenomenon induced by the operating temperature on the tested IMU has been investigated. More in detail, $D^{j}_{\text{Acc}}|_{@T_{\text{op}}}$ represents the data dispersion of the accelerometer j-axis at temperature T_{op} and it is evaluated as the median value of the point-by-point standard deviation of the movement acquisition $\sigma a^{j}_{T_{\text{op}}}$, which is determined with respect to the 30 identical test repetitions (all performed at the same temperature)

$$D^{j}_{\text{Acc}}\Big|_{@T_{\text{op}}} = \text{Med}\left(\sigma a^{j}_{T_{\text{op}}}\right). \tag{4}$$

Due to the possible presence of outliers resulting from the severe test conditions, the median has been used to increase the robustness of the analysis and avoid the influence of skewed data [36].

Similarly, $D^{j}_{\text{Gyro}}|_{@T_{\text{op}}}$ and $D^{j}_{\text{Mag}}|_{@T_{\text{op}}}$ represent the data dispersion at a temperature T_{op} along the j-axis of the gyroscope and magnetometer, respectively. Thus, they are evaluated as the median value of the standard deviation of the movement acquisition measured by the gyroscope $\sigma ar^{j}_{T_{\text{op}}}$ and by the magnetometer $\sigma m^{j}_{T_{\text{op}}}$, respectively

$$D^{j}_{\text{Gyro}}\Big|_{@T_{\text{op}}} = \text{Med}\left(\sigma ar^{j}_{T_{\text{op}}}\right) \tag{5}$$

$$D^{j}_{\text{Mag}}\Big|_{@T_{\text{op}}} = \text{Med}\left(\sigma m^{j}_{T_{\text{op}}}\right). \tag{6}$$

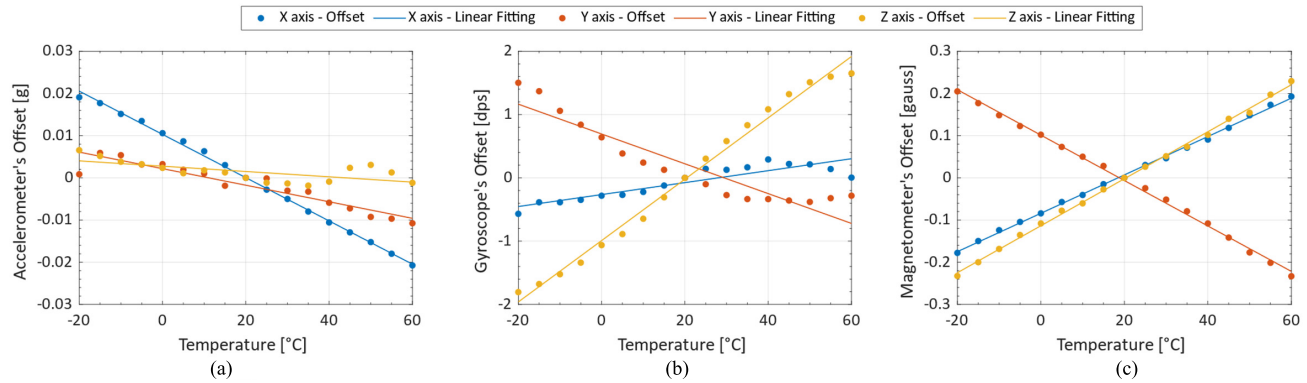

Fig. 7. Estimation of the offset $O^j_{\text{Acc}}|_{@T_{\text{op}}}$, $O^j_{\text{Gyro}}|_{@T_{\text{op}}}$, and $O^j_{\text{Mag}}|_{@T_{\text{op}}}$ during the dynamic test as a function of the operating temperature: observed values and linear fitting. (a) Accelerometer. (b) Gyroscope. (c) Magnetometer.

TABLE II

TEMPERATURE SENSITIVITY ANALYSIS OF THE IMU OUTPUT DURING DYNAMIC TEST: MAXIMUM OFFSET SWING, OFFSET SLOPE, AND GOODNESS OF FITTING OF THE LINEAR APPROXIMATION

AXIS	ACCELEROMETER			GYROSCOPE			MAGNETOMETER		
	OFFSET SWING	SLOPE OVER TEMPERATURE	R^2	OFFSET SWING	SLOPE OVER TEMPERATURE	R^2	OFFSET SWING	SLOPE OVER TEMPERATURE	R^2
X	0.040 g	-0.51 mg/°C	0.9979	0.859 dps	0.009 dps/°C	0.8085	0.371 gauss	4.55 mgauss/°C	0.9985
Y	0.017 g	-0.20 mg/°C	0.8848	1.883 dps	-0.024 dps/°C	0.8686	0.438 gauss	-5.38 mgauss/°C	0.9975
Z	0.008 g	-0.06 mg/°C	0.4340	3.456 dps	0.049 dps/°C	0.9901	0.462 gauss	5.57 mgauss/°C	0.9983

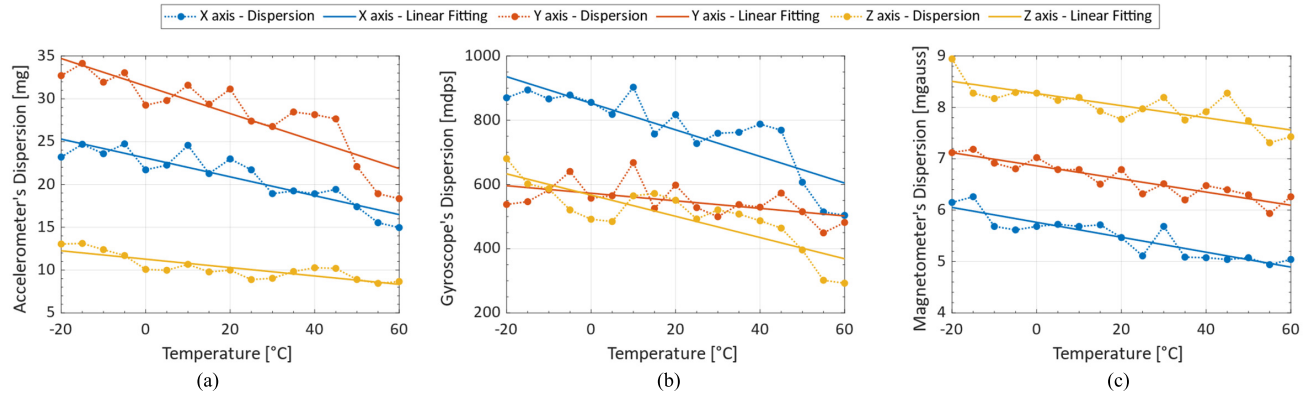

Fig. 8. Trend of the data dispersion during the dynamic test as a function of the operating temperature: observed values and linear fitting. (a) Accelerometer. (b) Gyroscope. (c) Magnetometer.

The data dispersion values estimated following (4)–(6) are illustrated in Fig. 8 as colored markers for every sensor [accelerometer in (a), gyroscope in (b), and magnetometer in (c)] and every axis.

In this case, analyzing the figure, it is possible to note a similar behavior to all sensors and all axes in terms of data dispersion as a function of the operating temperature. What stands out from the graphs is that the dispersion of the data measured acquiring the same movement at extremely cold temperatures is higher than the dispersion obtained at ambient and hot temperature conditions.

More specifically, a negative temperature dependence of the data dispersion has been encountered, with the magnitude of the slope in accordance with the different axes of the same sensor in almost all the analyzed cases. The only two exceptions are shown by the Z-axis of the accelerometer and the Y-axis of the gyroscope, which seems to point out an almost constant slope of the data dispersion.

TABLE III

DATA DISPERSION DEPENDENCE WITH TEMPERATURE: SLOPE IN CASE OF LINEAR FITTING FOR ALL IMU OUTPUTS

AXIS	ACCELEROMETER DISPERSION SLOPE	GYROSCOPE DISPERSION SLOPE	MAGNETOMETER DISPERSION SLOPE
X	-110.18 mg/°C	-4.14 mdps/°C	-14.52 mgauss/°C
Y	-160.58 mg/°C	-1.18 mdps/°C	-12.77 mgauss/°C
Z	-48.98 mg/°C	-3.31 mdps/°C	-11.82 mgauss/°C

To quantitatively analyze this aspect, Table III includes the slope of the first-degree polynomial fitting included in all subplots of Fig. 7 for every sensor and every axis. The table clarifies the negative sign for all the considered scenarios, showing a consistent dispersion increase in case of cold temperature conditions.

V. Conclusion

This work discusses about a dynamic characterization of a 9-DoF inertial measurement unit under thermomechanical conditions. Preliminary studies carried out in a static environment (i.e., maintaining the sensor platform in a fixed position) have pointed out a nonnegligible dependence between the IMU output and the operating temperature neglected by the manufacturer. Building upon this aspect, this article presented a customized experimental campaign to dynamically characterize the performances of the entire IMU in the presence of a harsh environment, which realistically emulates the installation on a motorcycle. For this reason, the IMU under test is installed on a rotation-producing device that is able to control and repeat the same identical movement for the sake of measurement repeatability. The equipment is located inside a climatic chamber to regulate the operating temperature, allowing the investigation and study of possible anomalies in a controlled environment. The initial qualitative analysis pointed out a dispersion of the measured data, changing the operating temperature in all sensors and all axes. For this reason, two customized metrics (the dynamic offset and the data dispersion) have been introduced in this article to quantitatively evaluate the impact that a change in the operating temperature could have on the IMU performances while measuring an actual movement. The results pointed out different temperature sensitivities of each sensor and axis regarding both magnitude and sign. Furthermore, a noticeable increase in the data dispersion has been found at cold temperatures. Overall, temperature variations can significantly affect IMU performances, and thus, temperature compensation becomes crucial for ensuring the accuracy of the IMU sensors. Common compensation techniques (e.g., polynomial regression or Kalman) and innovative approaches (e.g., adaptive filter and neural networks) will be introduced in future works to further extend the analysis using the data acquired during the combined dynamic temperature tests proposed in this work.

References

[1] L. Angrisani, P. Arpaia, A. Esposito, and N. Moccaldi, "A wearable brain-computer interface instrument for augmented reality-based inspection in industry 4.0," *IEEE Trans. Instrum. Meas.*, vol. 69, no. 4, pp. 1530–1539, Apr. 2020, doi: 10.1109/TIM.2019.2914712.

[2] G. D'Emilia, A. Gaspari, E. Natale, G. Adduce, and S. Vecchiarelli, "All-around approach for reliability of measurement data in the industry 4.0," *IEEE Instrum. Meas. Mag.*, vol. 24, no. 1, pp. 30–37, Feb. 2021, doi: 10.1109/MIM.2021.9345650.

[3] G. D'Emilia, A. Gaspari, and E. Natale, "Mechatronics applications of measurements for smart manufacturing in an industry 4.0 scenario," *IEEE Instrum. Meas. Mag.*, vol. 22, no. 2, pp. 35–43, Apr. 2019, doi: 10.1109/MIM.2019.8674633.

[4] J. Mindykowski and M. Savino, "An overview of the measurement of electrical quantities within imeko from 2003 to 2015," *Measurement*, vol. 95, pp. 33–44, Jan. 2017, doi: 10.1016/j.measurement.2016.09.040.

[5] A. Harindranath and M. Arora, "A systematic review of user–conducted calibration methods for MEMS-based IMUs," *Measurement*, vol. 225, Feb. 2024, Art. no. 114001, doi: 10.1016/j.measurement.2023.114001.

[6] S. Zihajehzadeh, T. J. Lee, J. K. Lee, R. Hoskinson, and E. J. Park, "Integration of MEMS inertial and pressure sensors for vertical trajectory determination," *IEEE Trans. Instrum. Meas.*, vol. 64, no. 3, pp. 804–814, Mar. 2015, doi: 10.1109/TIM.2014.2359813.

[7] Y. Xu et al., "A detection method for vortex precession frequency based on MEMS three-axis acceleration sensor," *IEEE Trans. Instrum. Meas.*, vol. 72, pp. 1–11, 2023, doi: 10.1109/TIM.2022.3224999.

[8] J. Abbasi, M. Hashemi, and A. Alasty, "A memory-based filter for long-term error de-noising of MEMS-gyros," *IEEE Trans. Instrum. Meas.*, vol. 71, pp. 1–8, 2022, doi: 10.1109/TIM.2022.3178964.

[9] J. Fu, Z. Ning, B. Li, and T. Lv, "Research on control algorithm of strong magnetic interference compensation for MEMS electronic compass," *Measurement*, vol. 207, Feb. 2023, Art. no. 112370, doi: 10.1016/j.measurement.2022.112370.

[10] Y. Cohen and A. Ya'akobovitz, "Comparative study on modeling approaches of V-shaped MEMS temperature sensors," *IEEE Trans. Instrum. Meas.*, vol. 68, no. 10, pp. 3766–3775, Oct. 2019, doi: 10.1109/TIM.2018.2879144.

[11] T. Jackson, K. Mansfield, M. Saafi, T. Colman, and P. Romine, "Measuring soil temperature and moisture using wireless MEMS sensors," *Measurement*, vol. 41, no. 4, pp. 381–390, May 2008, doi: 10.1016/j.measurement.2007.02.009.

[12] M. I. A. Asri, N. Hasan, M. R. A. Fuaad, Y. Yunos, and M. S. M. Ali, "MEMS gas sensors: A review," *IEEE Sensors J.*, vol. 21, no. 17, pp. 18381–18397, Sep. 2021, doi: 10.1109/JSEN.2021.3091854.

[13] I. Yoo et al., "Development of directional MEMS microphone single module for high directivity and SNR," *IEEE Sensors J.*, vol. 22, no. 7, pp. 6329–6335, Apr. 2022, doi: 10.1109/JSEN.2021.3127583.

[14] S. Park, J. Park, and C. G. Park, "Adaptive attitude estimation for low-cost MEMS IMU using ellipsoidal method," *IEEE Trans. Instrum. Meas.*, vol. 69, no. 9, pp. 7082–7091, Sep. 2020, doi: 10.1109/TIM.2020.2974135.

[15] J. Otegui, A. Bahillo, I. Lopetegi, and L. E. Díez, "Evaluation of experimental GNSS and 10-DOF MEMS IMU measurements for train positioning," *IEEE Trans. Instrum. Meas.*, vol. 68, no. 1, pp. 269–279, Jan. 2019, doi: 10.1109/TIM.2018.2838799.

[16] D. Capriglione et al., "Development of a test plan and a testbed for performance analysis of MEMS-based IMUs under vibration conditions," *Measurement*, vol. 158, Jul. 2020, Art. no. 107734, doi: 10.1016/j.measurement.2020.107734.

[17] D. Capriglione et al., "Experimental analysis of IMU under vibration," in *Proc. 16th IMEKO TC10 Conf.-Test., Diagnostics (Don't Short) Inspection Comprehensive Value Chain Quality Saf.*, Berlin, Germany, 2019, pp. 1–6.

[18] D. Capriglione et al., "Experimental analysis of filtering algorithms for IMU-based applications under vibrations," *IEEE Trans. Instrum. Meas.*, vol. 70, pp. 1–10, 2021, doi: 10.1109/TIM.2020.3044339.

[19] D. Capriglione et al., "Performance analysis of MEMS-based inertial measurement units in terrestrial vehicles," *Measurement*, vol. 186, Dec. 2021, Art. no. 110237, doi: 10.1016/j.measurement.2021.110237.

[20] P. Mohankumar, J. Ajayan, R. Yasodharan, P. Devendran, and R. Sambasivam, "A review of micromachined sensors for automotive applications," *Measurement*, vol. 140, pp. 305–322, Jul. 2019, doi: 10.1016/j.measurement.2019.03.064.

[21] H. Al Jlailaty, A. Celik, M. M. Mansour, and A. M. Eltawil, "IMU hand calibration for low-cost MEMS inertial sensors," *IEEE Trans. Instrum. Meas.*, vol. 72, pp. 1–16, 2023, doi: 10.1109/TIM.2023.3301860.

[22] M. Li, H. Zhu, S. You, and C. Tang, "UWB-based localization system aided with inertial sensor for underground coal mine applications," *IEEE Sensors J.*, vol. 20, no. 12, pp. 6652–6669, Jun. 2020, doi: 10.1109/JSEN.2020.2976097.

[23] Z. Zuo, B. Yang, Z. Li, and T. Zhang, "A GNSS/IMU/Vision ultra-tightly integrated navigation system for low altitude aircraft," *IEEE Sensors J.*, vol. 22, no. 12, pp. 11857–11864, Jun. 2022, doi: 10.1109/JSEN.2022.3168605.

[24] G. Patrizi et al., "Electrical characterization under harsh environment of DC–DC converters used in diagnostic systems," *IEEE Trans. Instrum. Meas.*, vol. 71, 2022, Art. no. 3504811, doi: 10.1109/TIM.2021.3129513.

[25] X. Zhao, G. Chen, H. Liu, and L. Wang, "A multivariate temperature drift modeling and compensation method for large-diameter high-precision fiber optic gyroscopes," *IEEE Trans. Instrum. Meas.*, vol. 71, pp. 1–12, 2022, doi: 10.1109/TIM.2022.3181900.

[26] M. Catelani, L. Ciani, A. Bartolini, C. Del Rio, G. Guidi, and G. Patrizi, "Reliability analysis of wireless sensor network for smart farming applications," *Sensors*, vol. 21, no. 22, p. 7683, Nov. 2021, doi: 10.3390/s21227683.

[27] Y. Günhan and D. Ünsal, "Polynomial degree determination for temperature dependent error compensation of inertial sensors," in *Proc. IEEE/ION Position, Location Navigat. Symp. - PLANS*, May 2014, pp. 1209–1212, doi: 10.1109/PLANS.2014.6851494.

[28] R. Fontanella, D. Accardo, R. S. Lo Moriello, L. Angrisani, and D. De Simone, "MEMS gyros temperature calibration through artificial neural networks," *Sens. Actuators A, Phys.*, vol. 279, pp. 553–565, Aug. 2018, doi: 10.1016/j.sna.2018.04.008.

[29] S. Chong et al., "Temperature drift modeling of MEMS gyroscope based on genetic-elman neural network," *Mech. Syst. Signal Process.*, vols. 72–73, pp. 897–905, May 2016, doi: 10.1016/j.ymssp.2015.11.004.

[30] B. Zhang, H. Chu, T. Sun, and L. Guo, "Thermal calibration of a tri-axial MEMS gyroscope based on Parameter-Interpolation method," *Sens. Actuators A, Phys.*, vol. 261, pp. 103–116, Jul. 2017, doi: 10.1016/j.sna.2017.04.013.

[31] Y. Zhang, L. Piao, and Y. Wang, "Compensation of temperature drift of micro gyroscope by polynomial fitting algorithm," in *Proc. IEEE 5th Inf. Technol.,Netw.,Electron. Autom. Control Conf. (ITNEC)*, vol. 5, Oct. 2021, pp. 307–310, doi: 10.1109/ITNEC52019.2021.9587304.

[32] Y.-H. Tu and C.-C. Peng, "An ARMA-based digital twin for MEMS gyroscope drift dynamics modeling and real-time compensation," *IEEE Sensors J.*, vol. 21, no. 3, pp. 2712–2724, Feb. 2021, doi: 10.1109/JSEN.2020.3028140.

[33] G. Betta et al., "Stress testing for performance analysis of orientation estimation algorithms," *IEEE Trans. Instrum. Meas.*, vol. 71, pp. 1–12, 2022, doi: 10.1109/TIM.2022.3216400.

[34] G. Patrizi et al., "Temperature stress tests on low-cost IMU systems: Analysis and first proposal for enhancing performance," in *Proc. IEEE Int. Instrum. Meas. Technol. Conf. (I2MTC)*, Ottawa, ON, Canada, May 2022, pp. 1–6, doi: 10.1109/I2MTC48687.2022.9806683.

[35] G. Patrizi, M. Carratù, L. Ciani, P. Sommella, M. Catelani, and A. Pietrosanto, "Analysis of inertial measurement units performances under dynamic conditions," *IEEE Trans. Instrum. Meas.*, vol. 72, pp. 1–13, 2023, doi: 10.1109/TIM.2023.3284957.

[36] S. Manikandan, "Measures of central tendency: Median and mode," *J. Pharmacol Pharmacother*, vol. 2, no. 3, pp. 214–215, 2011, doi: 10.4103/0976-500X.83300.

Gabriele Patrizi (Member, IEEE) received the master's degree (cum laude) in electronic engineering and the Ph.D. degree in industrial and reliability engineering from the University of Florence, Florence, Italy, in 2018, and 2022, respectively.

He is currently a Post-Doctoral Research Fellow of instrumentation and measurement and an Adjunct Lecturer of electric measurements with the University of Florence. In 2022, he joined the Institute of Electronic Packaging Technology (IAVT), Dresden Technical University, Dresden, Germany, as a Visiting Post-Doctoral Researcher. His research interests include life cycle reliability, condition monitoring for fault diagnosis of electronics, data-driven prognostic and health management, and instrumentation and measurement for reliability analysis.

Dr. Patrizi was a recipient of the "2023 Best Dissertation Award" from the IEEE IMS. He has been an Associate Editor of IEEE TRANSACTIONS ON INSTRUMENTATION AND MEASUREMENT (TIM) since 2023.

Marco Carratù (Member, IEEE) received the master's degree in electronic engineering and the Ph.D. degree from the University of Salerno, Fisciano, Italy, in 2015 and 2019, respectively.

He is currently an Assistant Professor of electronic measurements at the Department of Industrial Engineering, University of Salerno. His current research interests include instrument fault detection and isolation, sensor data fusion, digital signal processing for measurement instrumentation, artificial intelligence for instrumentation and measurement, and measurement uncertainty evaluation in machine learning techniques.

Dr. Carratù is an Associate Editor of IEEE OPEN JOURNAL OF INSTRUMENTATION AND MEASUREMENT (OJIM).

Lorenzo Ciani (Senior Member, IEEE) received the M.S. degree in electronic engineering and the Ph.D. degree in industrial and reliability engineering from the University of Florence, Florence, Italy, in 2005 and 2009, respectively.

He is currently an Associate Professor with the Department of Information Engineering, University of Florence. He has authored or coauthored more than 200 peer-reviewed journals and conference papers. His current research interests include system reliability, availability, maintainability and safety, reliability evaluation test and analysis for electronic systems and devices, fault detection and diagnosis, and electrical and electronic instrumentation and measurement.

Dr. Ciani is a member of the IEEE IMS TC-32 Fault Tolerant Measurement Systems. He received the 2015 IEEE I&M Outstanding Young Engineer Award for "his contribution to the advancement of instrumentation and measurement in the field of reliability analysis." He is an Associate Editor-in-Chief of IEEE TRANSACTION ON INSTRUMENTATION AND MEASUREMENT and an Associate Editor of IEEE ACCESS.

Paolo Sommella (Member, IEEE) was born in Salerno, Italy, in 1979. He received the M.S. degree in electronic engineering and the Ph.D. degree in information engineering from the University of Salerno, Fisciano, Italy, in 2004 and 2008, respectively.

In 2015, he joined the Department of Industrial Engineering (DIIn), University of Salerno, as an Assistant Professor of electrical and electronic measurements. His main interests are instrument fault detection and isolation, measurement in software engineering, and biomedical image processing.

Marcantonio Catelani (Member, IEEE) received the M.S. degree in electronic engineering from the University of Florence, Florence, Italy, in 1984.

He is currently with the Department of Information Engineering, University of Florence. Strictly correlated with reliability, availability, maintainability, and safety (RAMS) are the fields of interest of both fault diagnosis and reliability testing for components and equipment. In particular, the research activity concerns the development of test profiles used both for the characterization and the evaluation of reliability performance and, at the same time, the development of new degradation models able to estimate the life cycle of electronic components. His current research interests include the development of automatic measurement systems, the characterization of A/D converters, quality control and related statistical methods, and RAMS context.

Antonio Pietrosanto (Senior Member, IEEE) has been a Full Professor of instrumentation and measurement at the University of Salerno, Fisciano, Italy, since 2001. He has been a Founder of three spin-off companies of the University of Salerno: "SPRING OFF," "Metering Research," and "Hippocratica Imaging." His main research activities are in the fields of instrument fault detection and isolation (IFDIA), sensors, WSNs, real-time measurements, embedded systems, metrological characterization of measurement software, advanced system for food quality inspection, and image-based measurements. He has coauthored more than 150 papers in international journals and conference proceedings.

Dr. Pietrosanto is the today President of the Didactic Board of Electronic Engineering of UniSA.

Open Access funding provided by 'Università degli Studi di Firenze' within the CRUI CARE Agreement